On contact deflection and stiffness in spur and helical gears

Ph. Sainsot, Ph. Velex

On contact deflection and stiffness in spur and helical gears

Ph. Sainsot and Ph. Velex*

Revised version - July 2020

Université de Lyon, INSA Lyon, LaMCoS, UMR CNRS 5259,
Bâtiment Jean d'Alembert, 20 Avenue Albert Einstein,
69 621 Villeurbanne Cédex
France.

Philippe.Sainsot@insa-lyon.fr
Philippe.Velex@insa-lyon.fr

* Corresponding author
Tel.: +33 4 72 43 84 51
Fax: +33 4 78 89 09 80

Submitted for publication in Mechanism and Machine Theory.

Abstract:

A thorough review and analysis of the classic contact deflection formulae in gear simulations are presented. Based on extensive analytical developments, it is shown that the scatter in the results given by the classic formulations is mainly due to their respective displacement datum (either explicit or implicit) where contact deflections are supposed to vanish. Several formulae appear as not adapted to gears and a general formula for contact deflection or stiffness in gear teeth is proposed. A number of comparisons with 2D and 3D finite element results prove its validity and show that simplified thin-slice contact models give realistic results except near the edges of the contact lines.

Keywords: gear; contact deflection; contact stiffness; analytical formulae; finite element analysis.

1 - Introduction

Most of the elasticity models employed in gear simulations parallel the approach initially proposed by Weber [1-2] with the total tooth compliance decomposed into: a) the bending flexibility for the tooth assimilated to a cantilever beam or plate of variable thickness [2-6], b) the fillet and foundation contributions [1-3], [6-7] and, c) the local compliance at the contact [1-3, 6]. Although extensive finite element calculations are now routinely used, even for three-dimensional problems, lighter and faster models based on analytical or quasi-analytical results remain interesting particularly when extensive parameter analyses and/or dynamic analyses are required. A number of papers, only a few of which can be cited here [1-15], have dealt with the issues associated with tooth deflections and, if there is a global agreement on the modelling framework for structural deflections (bending and foundation), many contact deflection formulae can be found in the literature, which can lead to very contrasted results. It is therefore believed that a critical review of the various formulae for gear contact deflections is still of interest in order to clarify their respective underlying hypotheses and possible fields of application.

In the first section, several representative analytical formulations for contact deflections are derived using the elastic half-space theory and are commented upon. The corresponding orders of magnitude are then compared for realistic ranges of gear geometries and loading conditions. Some elements of explanation are proposed to account for the rather marked discrepancy between the results obtained by various formulae, suggesting that some of the classic contact compliance equations are not relevant for gears. Results are presented which, as far as the authors know, cannot be found in the open literature on gearing, and contribute to prove that, beyond their apparent disparity, a general form of tooth contact deflection formula can be formulated. In the second section, a number of comparisons with gear finite element models prove that the proposed analytical formulations are sound. Finally, the validity of a classic thin-slice model for three-dimensional simulations is analysed in the case not only of spur but also helical gears, where the contact lines are inclined on tooth flanks.

Nomenclature:

$$A = \frac{1}{2\bar{z}^2}\left[1 + \frac{\left(\bar{\ell} + \bar{y}\right)}{\sqrt{\left(\bar{\ell} + \bar{y}\right)^2 + \bar{z}^2}}\right]$$

b : half-width of contact (Figure 2)

c_0 : constant in the contact deflection formula ($-0.214 \le c_0 \le 0.148$ for steel gears)

E, E^* : Young's modulus, equivalent Young's modulus (as defined in (3))

h_a, h_f : addendum, dedendum coefficient

k : datum depth in the normal direction (Figure 5)

k_h : contact stiffness

k_{HS} : contact stiffness derived from Hamilton Standard formula [6], (33)

$k_{ys} = \dfrac{W}{2\Lambda} = \dfrac{\pi E(2\ell)}{4(1-\nu^2)}$, stiffness of reference

ℓ : half-length of contact (Figure 2)

m_0 : normal module (in mm)

$p_0, p(x,y) = p_0\sqrt{1-\dfrac{x^2}{b^2}}$: maximum contact pressure, contact pressure distribution

r_b, r_M, r : base radius, radius at point M (associated with α_M), pitch radius

R_1, R_2, R : radius of curvature of solid 1, solid 2, equivalent radius of curvature (3)

$w(0,y,z) = w_1(0,y,z) + w_2(0,y,z)$: vertical displacement at any point on the plane of symmetry $x = 0$ caused by a normal pressure distribution (1) (also Annex – section 1)

$w_0(x,y,z)$: vertical displacement at any point caused by a lumped force normal to the surface (2)

$W = p_0 \int_{-\ell}^{+\ell}\int_{-b}^{+b} \sqrt{1-\dfrac{x^2}{b^2}}\, dx\, dy$, total load

x : profile shift coefficient

$\overline{z}_L$: dimensionless datum depth for Lundberg's formula (approximate value)

Z, Z_1, Z_2 : tooth number, tooth number on pinion, tooth number on gear

α_0, α_M : pressure angle at pitch point, at any point of contact

β : helix angle

ε : precision for the definition of the datum depth for Lundberg's formula (14-15)

δ, δ_T : contact deflection for one solid, total contact deflection for two solids

$\Lambda = \dfrac{P_0 b}{2E^*} = \dfrac{W}{\pi E^*(2\ell)} = \dfrac{b^2}{4R}$, deflection of reference

$\eta = 1 + \sqrt{1+\dfrac{1}{\overline{z}^2}}$

ν : Poisson's ratio

Dimensionless variables

$\bar{X} = \dfrac{X}{b}$: variable normalised with respect to the half-contact width (X *is a generic variable*)

$\hat{X} = \dfrac{X}{\Lambda}$: variable normalised with respect to the deflection of reference (X *is a generic variable*)

2 - Analytical results

2-1 Three-dimensional analyses:

It is accepted that the characteristic dimensions of gear teeth are large compared with those of the contact area, so that the stresses and displacements can be calculated by considering each body as a semi-infinite elastic solid bounded by a plane surface, known as elastic half-space [16]. For standard lubrication conditions, friction forces can be neglected and the problem is reduced to finding the vertical displacements induced by a distribution of normal pressures applied to the contact area on the free surface.

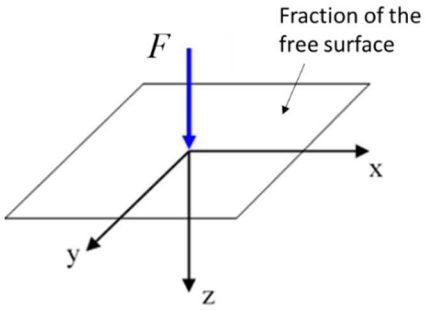

Figure 1- Lumped force perpendicular to the free surface of a half-space and coordinate system

Under the action of a normal concentrated force F at the origin of the coordinate system (Figure 1), the solution for the vertical displacement according to Boussinesq [17] reads:

$$w_0(x,y,z) = \frac{F(1+\nu)}{2\pi E}\left[\frac{z^2}{\left(x^2+y^2+z^2\right)^{3/2}} + \frac{2(1-\nu)}{\sqrt{x^2+y^2+z^2}}\right] \qquad (1)$$

from which, the total displacement induced by a normal pressure distribution $p(x', y')$ over a surface (S) can be found by superposition as:

$$w(x,y,z) = \frac{(1+\nu)}{2\pi E}\int_{(S)} p(x',y')\left[\frac{z^2}{\left((x-x')^2+(y-y')^2+z^2\right)^{3/2}} + \frac{2(1-\nu)}{\sqrt{(x-x')^2+(y-y')^2+z^2}}\right]dx'dy' \qquad (2)$$

A Hertzian pressure distribution over a rectangular strip $2b\times 2\ell$ (Figure 2) is considered as representative of the majority of the loading conditions in cylindrical gears, which reads:

$$p(x,y) = p_0\sqrt{1-\frac{x^2}{b^2}} \quad \text{when} \quad -\ell \le y \le \ell \quad \text{and} \quad -b \le x \le b$$
$$= 0 \qquad \text{otherwise} \tag{3}$$

with $b^2 = \dfrac{2WR}{\pi E^* \ell}$, b is the contact half-width,

$W = p_0 \int_{-\ell}^{+\ell}\int_{-b}^{+b} \sqrt{1-\dfrac{x^2}{b^2}}\, dx\, dy$, total load

$P_0 = \dfrac{W}{\pi b \ell}$, maximum contact pressure

$\dfrac{1}{E^*} = \dfrac{1-\nu_1^2}{E_1} + \dfrac{1-\nu_2^2}{E_2}$, equivalent Young's modulus

$\dfrac{1}{R} = \dfrac{1}{R_1} + \dfrac{1}{R_2}$, equivalent radius

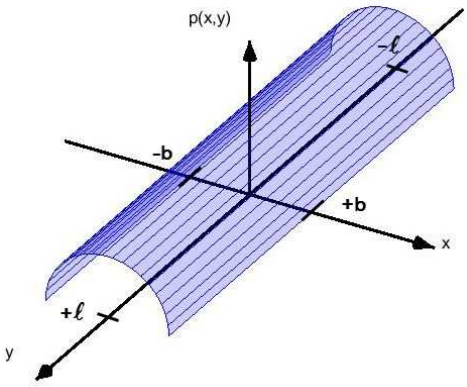

Figure 2 – Pressure distribution at the surface of an elastic half-space.

The analytical expressions and calculations can be simplified by using the following dimensionless variables:

$$\bar{y} = \frac{y}{b},\ \bar{z} = \frac{z}{b},\ \bar{\ell} = \frac{\ell}{b}$$
$$\hat{w}(.) = \frac{w(.)}{\Lambda} \tag{4}$$

where $\Lambda = \dfrac{P_0 b}{2E^*} = \dfrac{W}{\pi E^* (2\ell)} = \dfrac{b^2}{4R}$

$2\Lambda = \Lambda_1 + \Lambda_2 = \dfrac{b^2}{2R}$ represents the penetration depth between two elastic cylinders when the elastic couplings in the cylinders are ignored as illustrated in Figure 3 and, consequently, Λ can be viewed as the corresponding average deflection per solid.

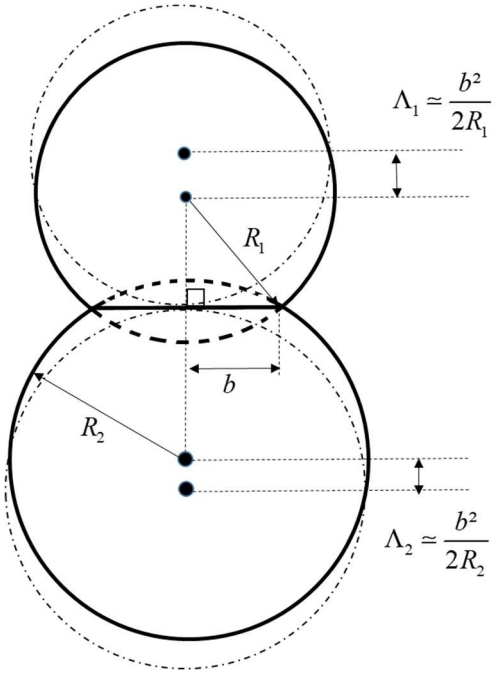

Figure 3 – Approach between two cylinders in contact when elastic couplings are ignored.

Direct integrations of (2) can be performed under certain conditions and, in what follows, only the displacements in the plane of symmetry $x = 0$ are presented, in accordance with the hypothesis of line contacts on tooth flanks.

a) At the surface of the loaded strip ($\overline{z} = 0$), a closed-form expression of the vertical displacement can be obtained providing that $\overline{\ell} - |\overline{y}| >> 1$ (hence, excluding the points close to the edges of the loaded area at $y = \pm \ell$) as:

$$\hat{w}(0, \overline{y}, 0) \approx \ln\left(2\overline{\ell}\right) + \frac{1}{2}\ln\left(1 - \left(\frac{\overline{y}}{\overline{\ell}}\right)^2\right) + 1.193 \qquad (5)$$

(see Annex, section 2, for the mathematical details)

from which, the classic Lundberg's formula [18] for the deflection at the centre of the contact is derived by setting $\overline{y} = 0$:

$$\hat{w}(0, 0, 0) \approx \ln\left(2\overline{\ell}\right) + 1.193 \qquad (6)$$

The expression of the vertical displacement at the edges of the contact can also be found to complement the previous formula since the exact integration at $y = \pm \ell$ leads to (Annex, section 3):

$$\hat{w}\left(0,\overline{y}=\pm\,\overline{\ell},0\right)=\frac{1}{2}\ln(2\,\overline{\ell})+0.943 \qquad (7)$$

b) for the same conditions (not too close to the contact edges at $y=\pm\,\ell$), the vertical displacement at a given depth $\overline{z}$ in the half-space is found to be (Annex, section 4) :

$$\hat{w}(0,\overline{y},\overline{z})=\frac{1}{2}\ln\left[\frac{\sqrt{\left(\overline{\ell}-\overline{y}\right)^2+\overline{z}^2}+\left(\overline{\ell}-\overline{y}\right)}{\sqrt{\left(\overline{\ell}+\overline{y}\right)^2+\overline{z}^2}-\left(\overline{\ell}+\overline{y}\right)}\right]+\ln(2)+\frac{1}{2}-\ln\left(1+\sqrt{1+A}\right)+\frac{1-\sqrt{1+A}}{A}$$
$$-\frac{1}{2(1-\nu)}\left[\frac{\overline{\ell}-\overline{y}}{\sqrt{\left(\overline{\ell}-\overline{y}\right)^2+\overline{z}^2}}+\frac{\overline{\ell}+\overline{y}}{\sqrt{\left(\overline{\ell}+\overline{y}\right)^2+\overline{z}^2}}\right]\left(\overline{z}^2-\overline{z}\sqrt{1+\overline{z}^2}\right) \qquad (8)$$

where $A=\dfrac{1}{2\overline{z}^2}\left[1+\dfrac{\left(\overline{\ell}+\overline{y}\right)}{\sqrt{\left(\overline{\ell}+\overline{y}\right)^2+\overline{z}^2}}\right]$

If $\overline{\ell}-\left|\overline{y}\right|>>\overline{z}>1$, (8) can be simplified and it gives a vertical displacement conveniently expressed as (Annex, section 5):

$$\hat{w}(0,\overline{y},\overline{z})\approx\hat{w}(0,\overline{y},0)-\ln\left(\eta\,\overline{z}\right)+\frac{\nu}{\eta\left(1-\nu\right)} \qquad (9)$$

with $\eta=1+\sqrt{1+\dfrac{1}{\overline{z}^2}}$

The validity of these analytical findings has been tested by comparisons with three-dimensional finite element results. An elastic parallelepipedic block (not shown) has been meshed with a very high node density in the vicinity of a rectangular strip loaded by a pressure distribution corresponding to (3). The block dimensions ($600\,b\times600\,b\times600\,b$) are far larger than the characteristic dimensions $2b\times30\,b$ of the loaded area in order to be close to the half-space conditions. The results in Figure 4 prove that the analytical developments and their underlying hypotheses are sound. The numerical and analytical displacements at the surface and at a dimensionless depth $\overline{z}=5$ are in excellent agreement. It can be observed that the surface deformed shape (in blue or blue squares) varies substantially with the *y*-coordinate, mainly near the edges of the contact area, which can be problematic if the displacement at the centre is considered as representative of the whole contact compliance, as is the case in Lundberg's formula. On the other hand, the relative deformed shape (displacements at the surface minus those at depth $\overline{z}=5$) is flat over the major part of the loaded area, which makes it possible to characterise the contact compliance by a single value. Finally, the approximate equation (9) gives $\hat{w}(0,\overline{y},0)-\hat{w}(0,\overline{y},\overline{z})\approx2.1$, which agrees very

well with the analytical and finite element results on the (extended) central part of the deformed line.

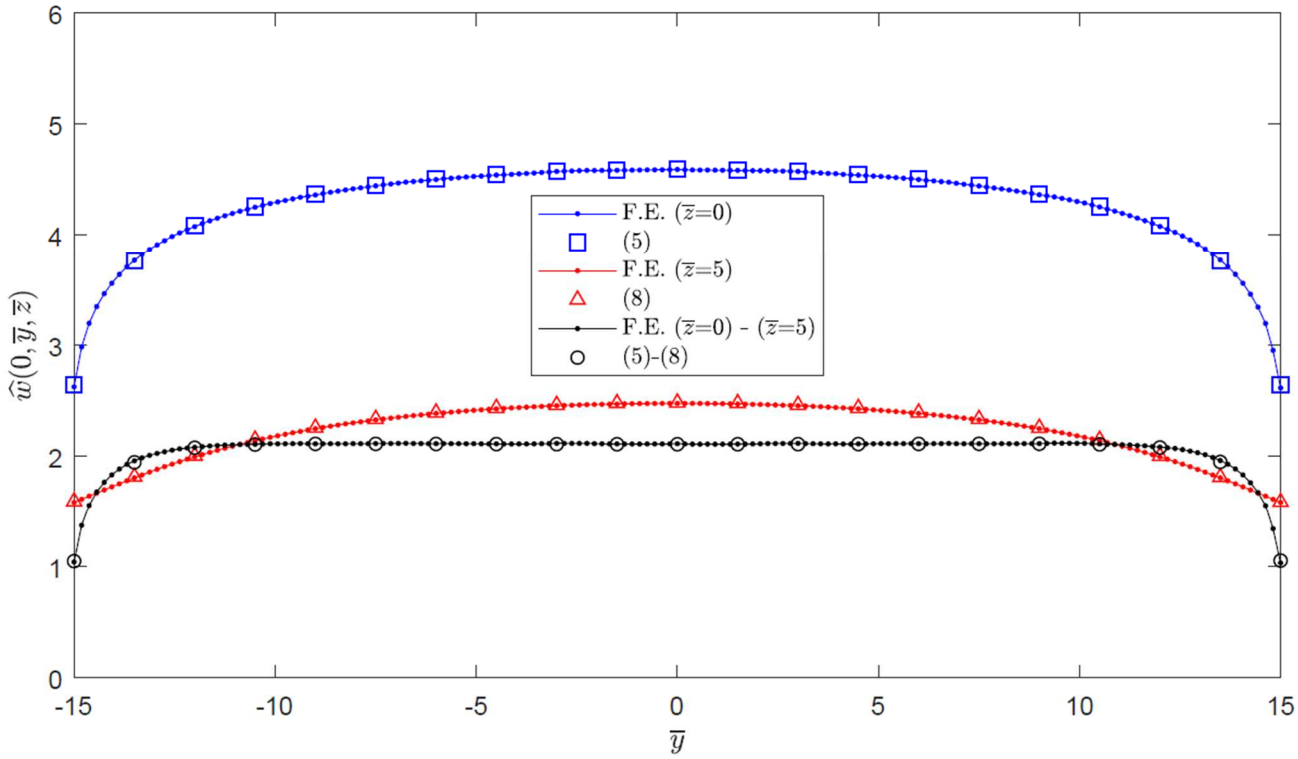

Figure 4 – Comparisons between FE results and half-space analytical formulae.
(*formula (6) was used for the two analytical deflections at the contact edges*).

Referring to the methodology introduced in [1-2] and employed by many researchers since, the decomposition into structural and contact deflections implies that the possible interactions between the two scales of analysis are discarded so that the total displacement is simply the sum of each individual contribution. In order to be applicable, this method implicitly imposes the contact displacement to be nil where bending displacement is considered, i.e., most of the time, at the intersection of the force line of action and tooth neutral fibre or surface. In this context, rather than the absolute displacement field at the surface, the relative displacements with respect to a datum line or surface need to be considered. From (9), a simple closed-form expression of such relative displacement is derived as:

$$\hat{\delta} = \overline{w}(0,\overline{y},0) - \overline{w}(0,\overline{y},\overline{z}) \approx \ln(\eta\,\overline{z}) - \frac{\nu}{\eta(1-\nu)} \qquad (10)$$

Based on these results, the following observations can be made:

a) For the central part of the line load, the difference between the deflection at the surface and that defined in (10) at any given depth $\overline{z}$ is nearly constant

(independent of y), making it possible to define a unique parameter representative of the contact flexibility,

b) If the datum depth is significantly larger than the contact half-length then $\eta \to 2$ and (10) takes the form of the classic bi-dimensional formula for the compression of a half-space relative to a point at depth $\overline{z}$ below the centre of a Hertzian contact pressure distribution [16]. Denoting the depth of reference $z = k$ and considering two contacting bodies (subscripts 1 and 2 respectively), the total contact deflection reads:

$$\hat{\delta}_T = \hat{\delta}_1 + \hat{\delta}_2 \; \ln\left(2\frac{k_1}{b}\right) + \ln\left(2\frac{k_2}{b}\right) - \frac{\nu}{(1-\nu)} = 2\left[\ln\left(2\frac{\sqrt{k_1 k_2}}{b}\right) - \frac{\nu}{2(1-\nu)}\right] \quad (11)$$

which, when re-introducing the physical parameters, takes the form:

$$\delta_T = 4\frac{W}{(2\ell)}\frac{(1-\nu^2)}{\pi E}\left[\ln\left(2\frac{\sqrt{k_1 k_2}}{b}\right) - \frac{\nu}{2(1-\nu)}\right] \quad (12)$$

In the field of gearing, (12) is known as Weber-Banaschek's formula [1-2,6], providing that the datum depth *k* corresponds to the intersection of the tooth centre line and the contact force line of action as shown in Figure 5.

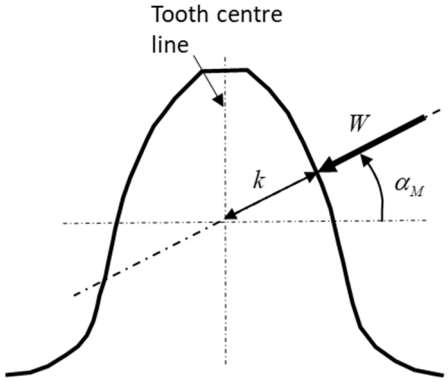

Figure 5 – Datum for contact displacements in [1-2]

c) For three-dimensional half-spaces, the displacements shrink to zero for points far from the loaded surface (as opposed to two-dimensional half-planes), which reveals that the compliance given by Lundberg's formula (6) must always be larger than that derived from Weber-Banaschek's equation (11). Considering Lundberg's formula, an order of magnitude of the datum depth $\overline{z}_L$, where vertical displacements can be neglected, is derived by supposing that $\frac{\overline{z}_L}{\overline{\ell}} \gg 1$ and $\frac{1}{\overline{z}_L} \ll 1$. In these conditions, the displacement $\hat{w}(0, \overline{y}, \overline{z})$ in (8) can be linearized and keeping the value at the centre of the contact zone $\overline{y} = 0$, one obtains:

$$\hat{w}(0,0,\overline{z}) \approx \frac{3-2\nu}{2(1-\nu)}\left(\frac{\overline{\ell}}{\overline{z}}\right) \qquad (13)$$

The datum depth can be approximated using the following inequality:

$$\hat{w}(0,0,\overline{z}_L) \le \varepsilon\, \overline{w}(0,0,0) \qquad (14)$$

where ε is a percentage below which the difference in displacement can be ignored in practice.

For $\nu = 0.3$, (14) leads to:

$$\overline{z}_L \ge \frac{1.714}{\varepsilon} \frac{\overline{\ell}}{\left[\ln\left(2\overline{\ell}\right)+1.193\right]} \qquad (15)$$

d) After some manipulations, it appears that formula (10) also gives the maximum compression of an infinite elastic slab of large thickness $\overline{z}$ compared with the contact length *2b*, submitted to a semi-elliptic pressure field [19],

Finally, concerning three-dimensional models, the half-space approximation for gear teeth is certainly questionable in the axial direction, since the contact zone usually extends over the entire face width, and the influence of edge effects on contact deflections has to be assessed. To this end, a smaller block of dimensions $600b \times 30b \times 600b$ is simulated by 3D finite elements so that one dimension corresponds to the loaded length (same loaded area as that leading to the results in Figure 4). The results in Figure 6 prove that, compared with the half-space results, the overall contact compliance is increased by a factor of nearly 2 with more deflection near the free edges (as opposed to what is observed in Figure 4). However, it is also noticed that the relative displacement curve between the surface and depth $\overline{z} = 5$ is still well represented using the difference between the displacements in (5) and (8), suggesting that formula (10) remains valid even for finite width solids.

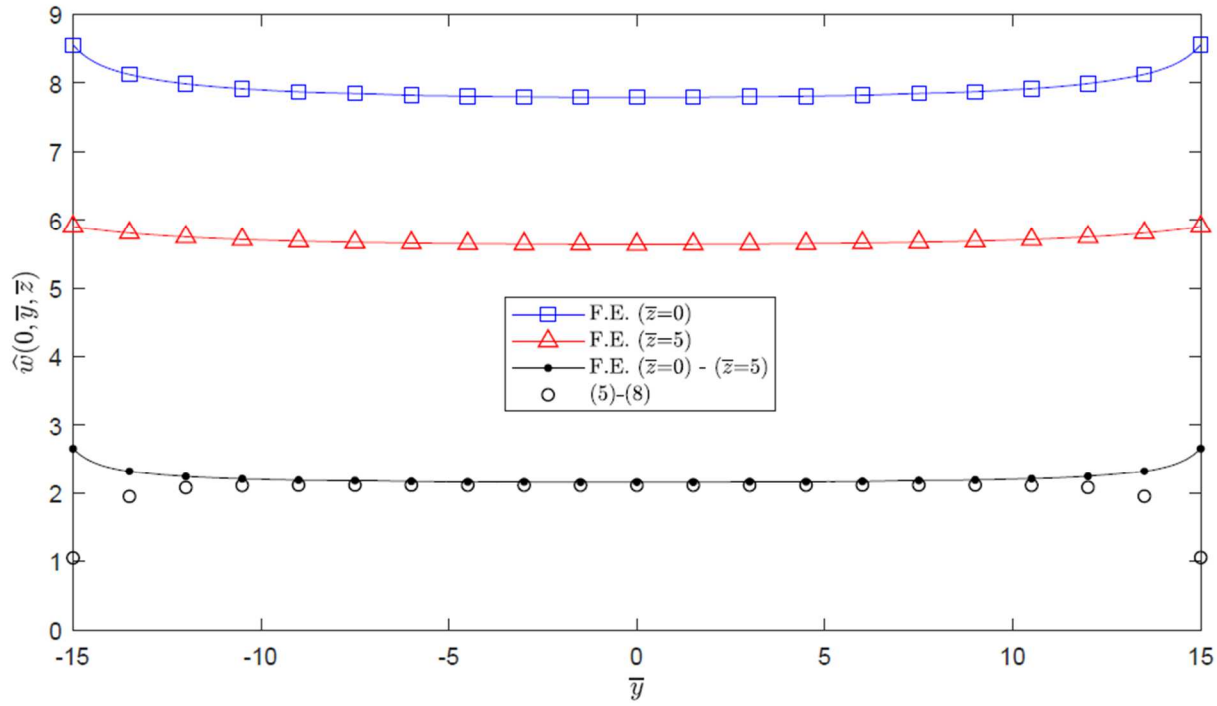

Figure 6. – Comparisons between FE results and the analytical formulae for a block.
Eq. (10) gives $\hat{\delta} \approx 2.1$ *in good agreement with the numerical and analytical formulae.*

2-2 Bi-dimensional formulae - Other formulae

Different formulae can be found in the literature, which stem from bi-dimensional models in the $(O,\mathbf{x},\mathbf{z})$ plane. Considering elastic half-planes, the Hertz theory relates the load per unit of face width $W/2\ell$ to the contact width *2b* but no corresponding result can be given for the contact deflection (approach). The displacements of points in the contact area with respect to a datum, increase indefinitely with the datum depth (as indicated by (15) when $\overline{\ell} \to \infty$ would correspond to the bi-dimensional situation). For a state of plane strains and supposing that the vertical displacement vanishes at a depth $z = k$ under the origin (centre of the pressure distribution), one obtains equation (10) with $\eta = 2$ [16]. An alternative modelling strategy consists in replacing the elastic half-plane by a slab of infinite dimension in the *x*-direction, whose thickness (in the *z*-direction) is larger than the contact width *2b*. In the case of an infinite elastic layer of depth $\overline{z} = \overline{k}$ attached to a rigid base and indented by a rigid circular cylinder of radius *R* on its free surface (Figure 7), the vertical displacement at the centre of the contact according to Meijers [20] can be expressed, for a Poisson's ratio $\nu = 0.3$, as:

$$\hat{\delta} = \ln\left(2\overline{k}\right) - 0.0268 \qquad (16)$$

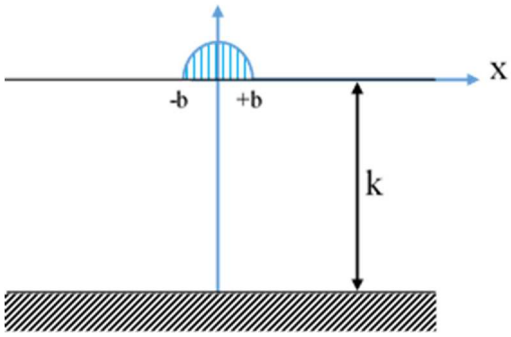

Figure 7- Elastic slab parameters and loading.

Greenwood *et al.* [21-22] have proposed a new mathematical solution for a semi-infinite slab resting on a rigid frictionless base and indented by a rigid cylinder of radius R leading, for $\nu = 0.3$, to the following contact deflection:

$$\hat{\delta} = \ln\left(2\bar{k}\right) + 0.14832 \qquad (17)$$

The two slab formulae (16) and (17) along with the proposed equation (10) (hence, Weber & Banaschek's formula (11-12)) have very similar structures although the constant term can either be positive or negative but also dependent on Poisson's ratio or not (as already pointed out by Greenwood and Barker [22]). In practice, however, these variations are of limited influence since the ratio $\bar{k}$ in most gears is such that the logarithmic term is dominant with possible exceptions near tooth tips nonetheless.

In 1981, Cornell [6] published an approximate formula for the total contact deflection (whose exact origin remains unclear to the authors) initially developed at Hamilton Standard. Assuming that each contacting solid contributes to approximately half of the total contact deflection, it leads to the following order of magnitude for the individual contact deflection:

$$\hat{\delta} \approx (2 + \frac{\pi}{2}) \approx 3.57 \qquad (18)$$

A very popular equation for contact stiffness in gears (Yang and Sun [23]) is used in a number of papers [24-28]. It is similar to the formula proposed by Popov [29] in the qualitative analysis of the contact between an elastic cylinder and a rigid plane and based on modelling hypotheses corresponding to the situation shown in Figure 3. Under the same hypothesis as for (18), (half of the contact deflection attributed to each solid in contact), it gives the contact deflection for one solid as:

$$\hat{\delta} \approx 1 \qquad (19)$$

The empirical relationship proposed by Palmgren [30] for a steel cylinder compressed between two elastic platens can be adapted to derive the deflection of one contacting body as:

$$\delta = 1.905\left(\frac{\Lambda}{2}\right)^{0.9}\left(2\ell\right)^{0.1} \text{ (SI units)} \qquad (20\text{-}1)$$

$$\hat{\delta} = 2.042\left(2\bar{R}\,\bar{\ell}\right)^{0.1}, \text{ dimensionless form with } \bar{R} = \frac{R}{b} \qquad (20\text{-}2)$$

or alternatively

$$\hat{\delta} \approx 27.34\left(\frac{W}{2\ell}\right)^{-0.1}(2\ell)^{0.1} \qquad (20\text{-}3)$$

Finally, for geometrical and loading conditions close to Palmgren's empirical formula, it is worth mentioning the theoretical expression for the deflection of a half-cylinder submitted to a Hertzian pressure distribution (Johnson [16]), which reads:

$$\hat{\delta} = \ln\left(2\bar{R}\right) + 0.193 \qquad (21)$$

2-3 Synthesis

Table 1 synthetises the deflection formulae presented in the previous sections for one contacting body assuming that the material is steel ($E = 2.07\,\text{GPa}$ $\nu = 0.3$).

Reference -	Formula	Equation
Proposed formula - SV	$\hat{\delta} \approx \ln\left(\eta\bar{k}\right) - \frac{0.429}{\eta}$ with $\eta = 1 + \sqrt{1 + \frac{1}{\bar{k}^2}}$	(10)
Weber-Banaschek – WB [1-2]	$\hat{\delta} = \ln\left(2\bar{k}\right) - 0,214$	Same as (10) with $\eta = 2$
Meijers - M [20]	$\hat{\delta} = \ln\left(2\bar{k}\right) - 0,027$	(16)
Greenwood-Barber - GB [21-22]	$\hat{\delta} = \ln\left(2\bar{k}\right) + 0.148$	(17)
Hamilton Standard - HS [6]	$\hat{\delta} \approx 2 + \frac{\pi}{2} \approx 3.57$	(18)
Yang-Sun and Popov – YS-P [23] and [29]	$\hat{\delta} \approx 1$	(19)

Lundberg - L [18]	$\hat{\delta} \approx \ln\left(2\bar{\ell}\right)+1.193$	(6)
Palmgren - P [30]	$\hat{\delta}=2.042\left(2\bar{R}\,\bar{\ell}\right)^{0.1}$ $\approx 27.34\left(\frac{W}{2\ell}\right)^{-0.1}\left(2\ell\right)^{0.1}$	(20)
Johnson – J [16]	$\hat{\delta}=\ln\left(2\bar{R}\right)+0.193$	(21)

Table 1 – Contact deflection formulae – Synthesis.

2-4 Orders of magnitude and ranges of variation

The relevant groups of parameters in the contact deflections formulae listed in Table 1 are mainly $\bar{k}=\frac{k}{b}$, $2\bar{\ell}=\frac{2\ell}{b}$ and $\bar{R}=\frac{R}{b}$, whose orders of magnitude need to be determined for quantitative comparisons.

a) The distance k to the tooth centre-line in the normal direction with respect to the tooth profile (Figure 5) can be expressed as:

$$\frac{k}{m_o}=\frac{Z}{2}\cos\left(\alpha_o\right)\left\{\tan\left(\alpha_M\right)-\tan\left[\tan\left(\alpha_M\right)-\frac{\theta_b}{2}\right]\right\} \qquad (22)$$

where

$$\theta_b=\frac{2}{Z}\left[\frac{\pi}{2}+2x\tan\left(\alpha_o\right)\right]+2inv\left(\alpha_o\right)$$

$$\alpha_M=a\cos\left(\frac{r_b}{r_M}\right)$$

(*See the nomenclature for the parameter definition*)

No closed form has been found for *k* but systematic sweeps over realistic ranges of variables can be easily conducted whose results are shown in Figure 8 for a standard pressure angle of 20°, tooth numbers in the range [15 -150] and profile shift coefficients of -0.5, 0, +0.5. From the figure, it can be concluded that:

$$0.3\le\frac{k}{m_o}\le 1.2 \qquad (23)$$

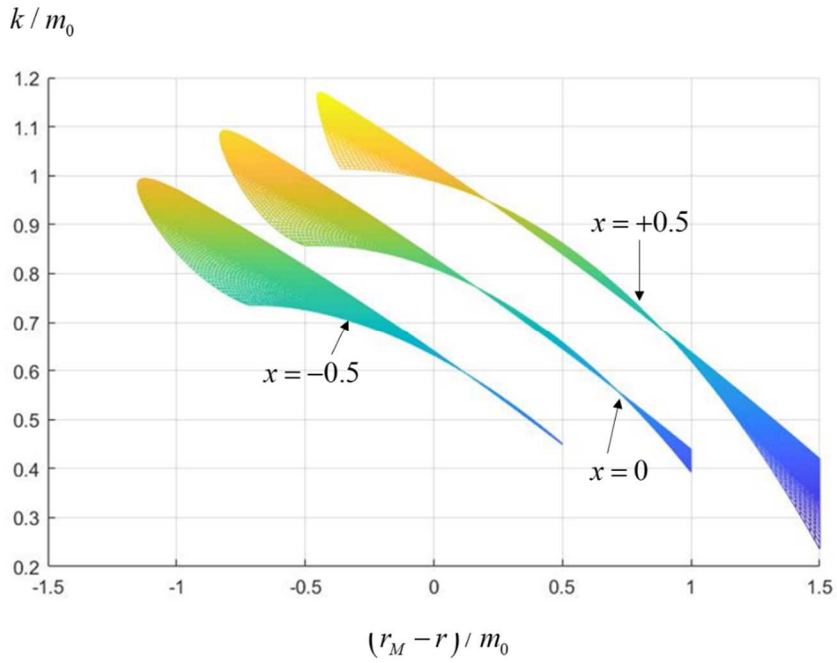

Figure 8 - k/m_0 for a range of tooth numbers and three profile shift coefficients.

b) Orders of magnitude can be derived for the equivalent radius of curvature R which,

at the pitch point, is given by $\frac{R}{m_0} = \frac{\sin(\alpha_o)}{2}\left[\frac{1}{Z_1} + \frac{1}{Z_2}\right]^{-1}$ in the absence of profile shift.

For the conditions listed above and assuming that $18 \le Z_1 \le 45$ and $18 \le Z_2 \le 150$, one obtains:

$$1.53 \le \frac{R}{m_o} \le 5.96 \qquad (24)$$

c) Limits for the contact half-width b can be found for steel gears and realistic loads per unit of contact length $\frac{W}{2\ell}$ in gears between 100 N/mm and 300 N/mm as:

$$\frac{0.041}{\sqrt{m_0}} \le \frac{b}{m_0} \le \frac{0.141}{\sqrt{m_0}} \qquad (m_0 \text{ in mm}) \qquad (25)$$

d) The typical range for face widths (or contact lengths here) is such that:

$$5 \le \frac{2\ell}{m_0} \le 20 \qquad (26)$$

Finally, for the ranges of geometry and loads considered above, the following bounds of variations are derived:

$$
\begin{aligned}
&4.25\sqrt{m_0} \le 2\bar{k} \le 29.27\sqrt{m_0} \\
&28.35\sqrt{m_0} \le 2\bar{\ell} \le 487.8\sqrt{m_0} \\
&21.69\sqrt{m_0} \le 2\bar{R} \le 290.7\sqrt{m_0} \\
&(m_0 \text{ in mm})
\end{aligned}
\qquad (27)
$$

which, when re-injected in the analytical expressions in Table 1, makes it possible to define the bounds of variation given by the various contact deflection formulae in Table 2.

A number of conclusions can be drawn from the results in Table 2:

a) YS-P formula (19) leads to substantially lower deflections about 2-3 times smaller on average than those obtained by all the other equations in this survey.

b) 2 groups of formulae can be distinguished:

- WB-SV (10), M (16), GB (17), which, for typical modules between 1 and 10 mm, lead to average dimensionless deflections around 2.9– 3.3, i.e., the same order of magnitude as the Hamilton Standard formula HS (18).
- L (6), P (20), J (21), which give rise to larger average deflection amplitudes more adapted to elastic cylinders and commonly used in roller bearing design, thus relying on a deeper displacement datum equal to the cylinder radius R (hence far larger than k). From a deflection viewpoint, a tooth cannot be assimilated to a cylinder in contrast to what is often assumed to define the local geometry at the contact. The good agreement between (20) and (21) is to be noted.

c) The compliances derived from semi-infinite slab formulations M (16), GB (17), are slightly higher than those from semi-infinite elastic media based on a displacement datum or relative displacement WB-SV (10).

Reference	Limits for $1 \le m_0 \le 10$ (m_0 in mm)
Proposed formula – SV and Weber-Banaschek - WB [1-2]	$1.23 \le \hat{\delta} \le 4.31$
Meijers - M [20]	$1.42 \le \hat{\delta} \le 4.5$
Greenwood-Barber - GB [22]	$1.59 \le \hat{\delta} \le 4.68$

Hamilton Standard - HS [6]	$\hat{\delta} \approx 3.57$
Yang-Sun and Popov – YS-P [23], [29]	$\hat{\delta} \approx 1$
Lundberg - L [18]	$4.53 \leq \hat{\delta} \leq 8.53$
Palmgren - P [30]	$3.62 \leq \hat{\delta} \leq 6.24$
Johnson – J [16]	$3.27 \leq \hat{\delta} \leq 7.01$

Table 2 – Realistic ranges of variation for various contact deflection formulae.

Conditions: steel gears ($E = 2.07\,10^{11}$ Pa, $\nu = 0.3$*), standard pressure angle* $\alpha_0 = 20°$*, load per unit contact width between 100 and 300 N/mm, face-widths between 5 and 20 modules, tooth numbers between 15 and 150, modules between 1 and 10 mm.*

Figure 9 shows comparisons between the various deflection formulae and reveals a remarkable continuity between all the formulations, providing that the datum range is sufficiently large (variation approximately proportional to $\ln(\bar{k})$). This remark highlights the fact that contact deflections do not necessarily vanish at points on the tooth centre-line as implicitly assumed in the approaches superimposing contact, tooth bending and foundation displacements. It is also confirmed that L (6) represents the asymptotic limit of the difference between (5) and (8) when the datum depth increases.

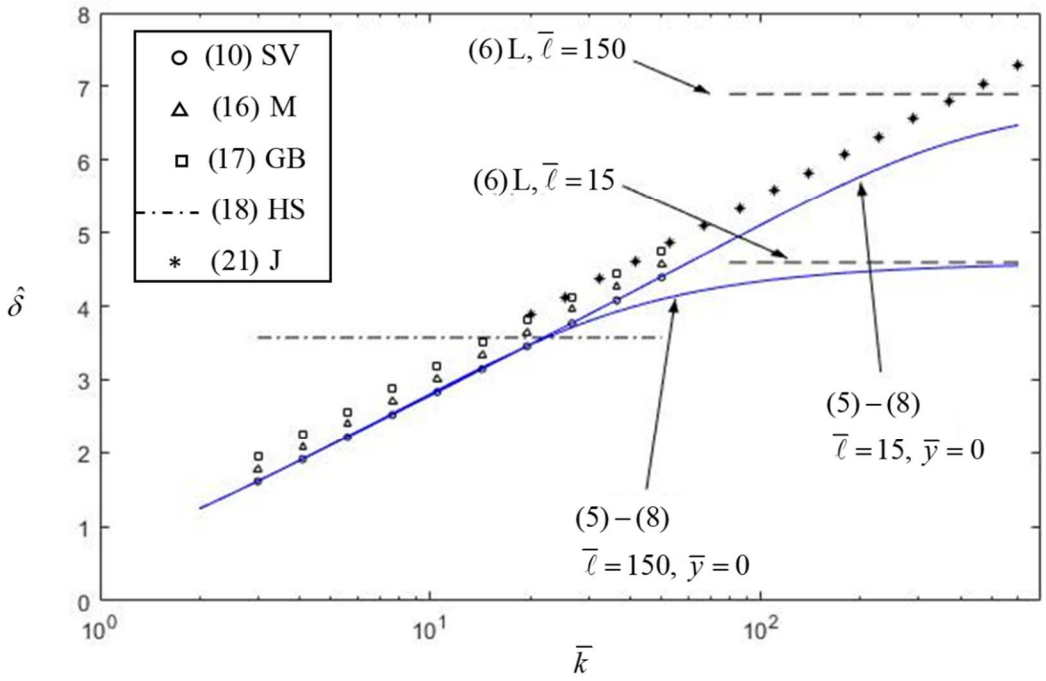

Figure 9 – Comparisons between several analytical formulae over a broad range of dimensionless datum depths $\overline{k}$

2– Comparisons with results from finite element models

2.1 Two-dimensional models

The finite element model of three consecutive teeth in Figure 10 is used to calculate the contact deflections on realistic tooth geometries (Table 3) as opposed to the semi-infinite elastic media employed in the analytical formulations. Only the central tooth is loaded in order to minimise the influence of the boundary conditions and the node density on its profile is adjusted so that a Hertzian semi-elliptical pressure distribution can be directly applied (Table 3). Adaptive meshing ensures that the highly refined grid always matches with the loaded area as it is displaced along the profile. Note that the load and contact width b are kept constant and that the transition between one and two tooth pairs in contact is not simulated.

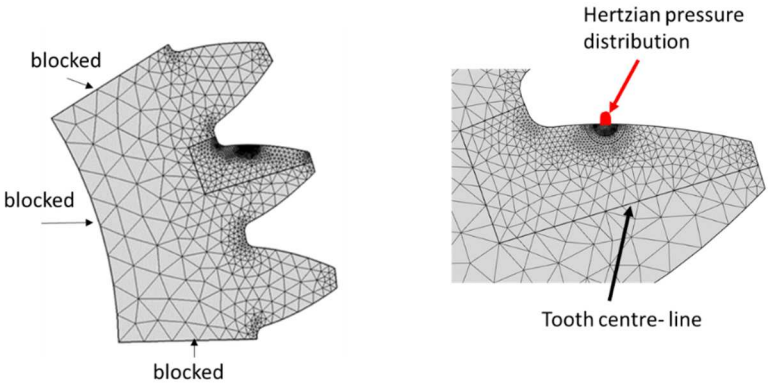

Figure 10 – 2D finite element model.

Z	m_0 (mm)	α_0 (°)	β (°)	h_a	h_f	x		p_0 (GPa)	b (mm)
25	2	20	0	1	1.25	0		1.34	0.12
			10					1.30	0.12
			30					1.23	0.16

Table 3 – Gear data and loading conditions

In accordance with the analytical findings, the difference between the displacements in the load direction *i*) at the contact centre and, *ii*) at the intersection between the load line of action and tooth centre line, has been calculated for several positions from the tooth tip to the root. Figure 11 shows the corresponding results versus the position of the load on the profile and proves that the selected formulations agree generally well with the numerical values. The finite element results lie between the displacement curves given by M (16) and GB (17), whereas the deflections based on WB-SV (10) are systematically lower.

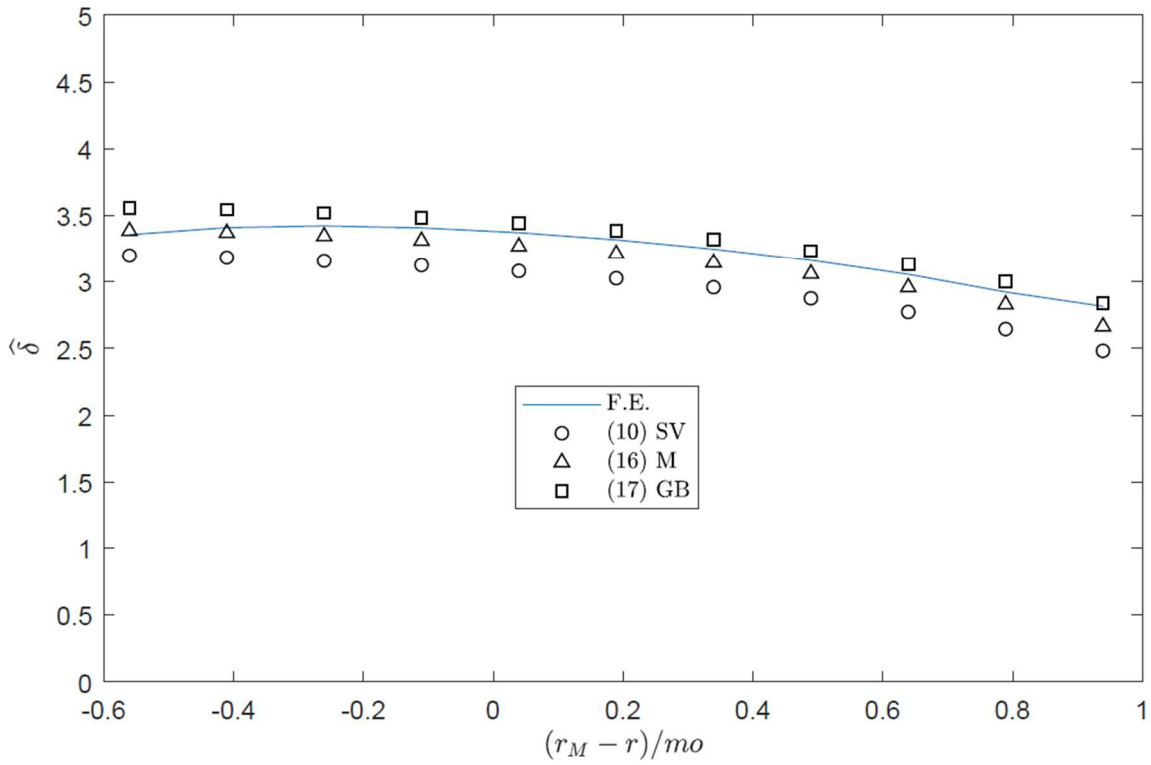

Figure 11 – Comparisons between FE and analytical results at various positions on the tooth profile.

2.2 Three-dimensional models

The 3D finite element model for one spur gear tooth is shown in Figure 12-a. The displacements are blocked at the three interfaces with the gear body and only the limits of the various sub-domains in terms of node density are represented. Figure 12-b shows all the nodes in the FE model whereas Figure 12-c represents the node distribution over and near the loaded

area showing that a semi-elliptical Hertzian pressure distribution can actually be accounted for with enough precision. The node density is, in fact, comparable to that used for the blocks (leading to the results in Figures 4 and 6), which was proved accurate enough as it gave the same deflections as the theoretical results for a loaded elastic half-space. The pressure distribution is applied on the highest node density zone centred on the intersection between the pitch cylinder and the tooth flank. The datum deflections are the displacements in the force direction (normal to tooth flank) on the line defined as the intersection between the tooth mid-surface and the base plane. In order to reproduce the analytical conditions, the contact deflections are then calculated as the differences between the normal surface displacements along the centre line of the loaded zone and the datum deflections.

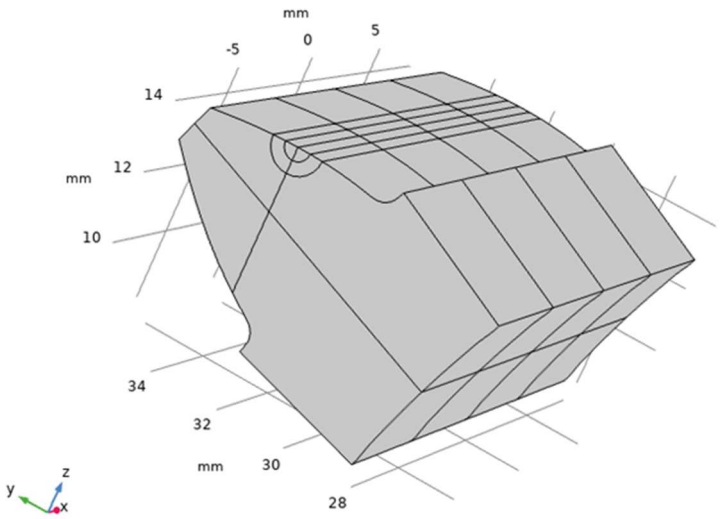

a) Different subdomains in the FE grid

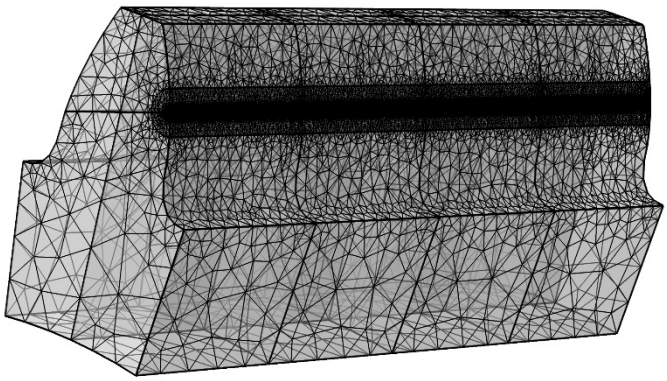

b) Representation of all the nodes – Entire tooth

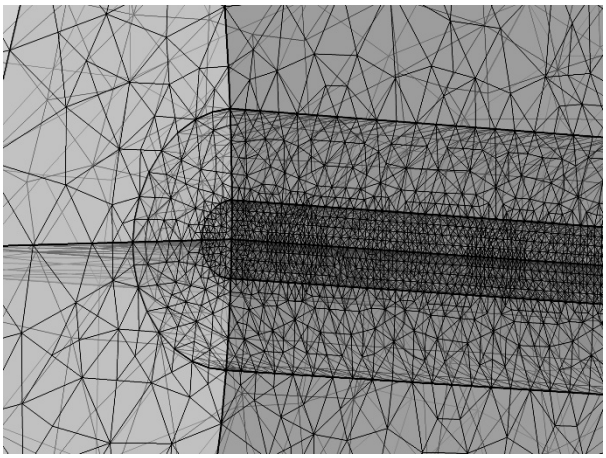

c) Node density near the loaded area (detail of figure 12 – b above). The highest density surface corresponds to the loaded area on tooth flank.

Figure 12 – 3D finite element model – Spur gear example.

On the other hand, the analytical deflections are derived from a classic thin-slice approach whereby two-dimensional results can be extended to line contacts sliced into a number of independent equal segments across the face width, each of them being dealt with as a 2D contact of width equal to the segment length.

Considering, first, a uniform pressure distribution, the results in Figure 13 show the contact deflection distribution in the face width direction and prove that the 3D finite element and analytical results (especially the Greenwood & Barber formula (21-22)) agree well. As expected, however, more deviations are noticed close to the tooth edges, in line with the observations on elastic convectivity and thin-slice models in [31-32].

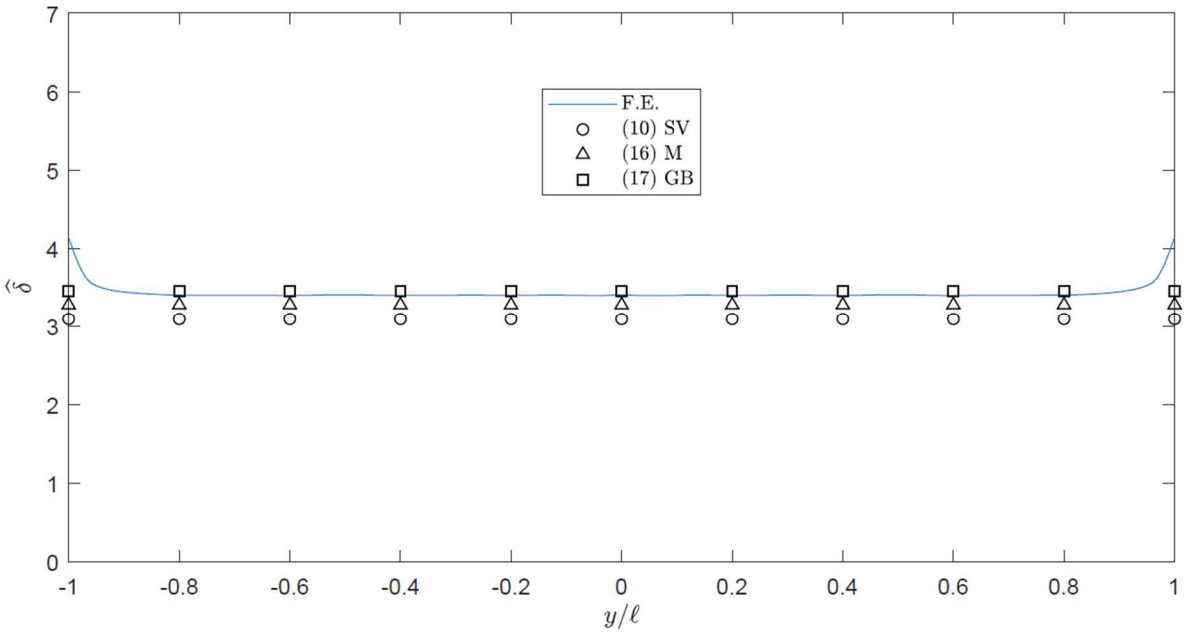

Figure 13 – Comparisons between 3D FE and analytical results across the face width for a uniform load distribution at a height corresponding to the pitch radius. Spur gear example.

The second set of results in Figs. 14 and 15 corresponds to non-uniform axial load distributions namely, a linear and a cosine variation, aimed at simulating large misalignments and lead crowns, of the form:

$$W_L(y) = W_0(1-0.95\bar{y})$$
$$W_C(y) = W_0(1+0.95\cos(\pi\bar{y})) \qquad (28)$$

with $-1 \le \bar{y} \le 1$ and $W_0 = 252 N/mm$

In these cases, both the contact width *b* and maximum pressure p_0 vary and have been adjusted based on the local load on each slice. For the linear load variation across the face-width, the thin-slice and finite element results are still in good agreement (except at the edges), whereas more discrepancies can be noticed for the cosine load variation. For the latter, larger differences are visible near the flank edges, thus highlighting the limitations of thin-slice models when tooth loading is neither constant nor linear. This observation is consistent with the findings in [31-32] proving that the influence of couplings between adjacent slices are of secondary importance as long as the curvature induced by deflections in the contact line direction can be neglected. For other cases, more deviations are to be expected, although the analytical and finite element deflection curves in Fig. 15 remain reasonably close in the central part of the loaded area. Although relative deviations as high as 25% can be observed close to the edges, their influence on the global behaviour remains limited and compatible with dynamic models, which are mainly dependent on global mesh properties.

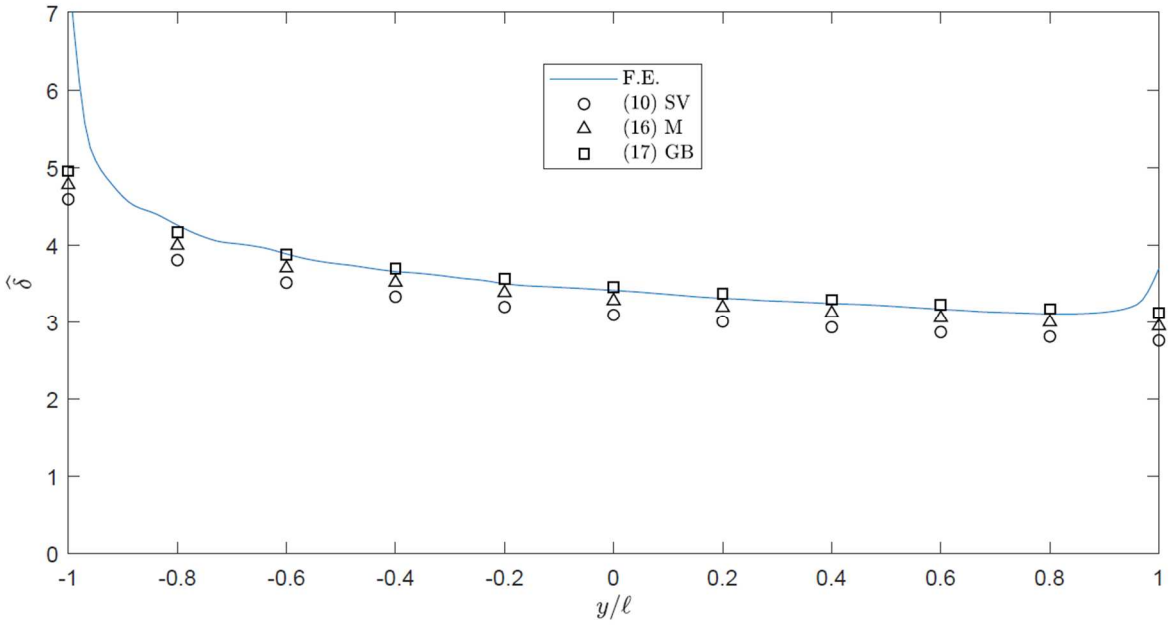

Figure 14 - Comparisons between 3D FE and analytical results across the face width for a linear load distribution at a height corresponding to the pitch radius. Spur gear example.

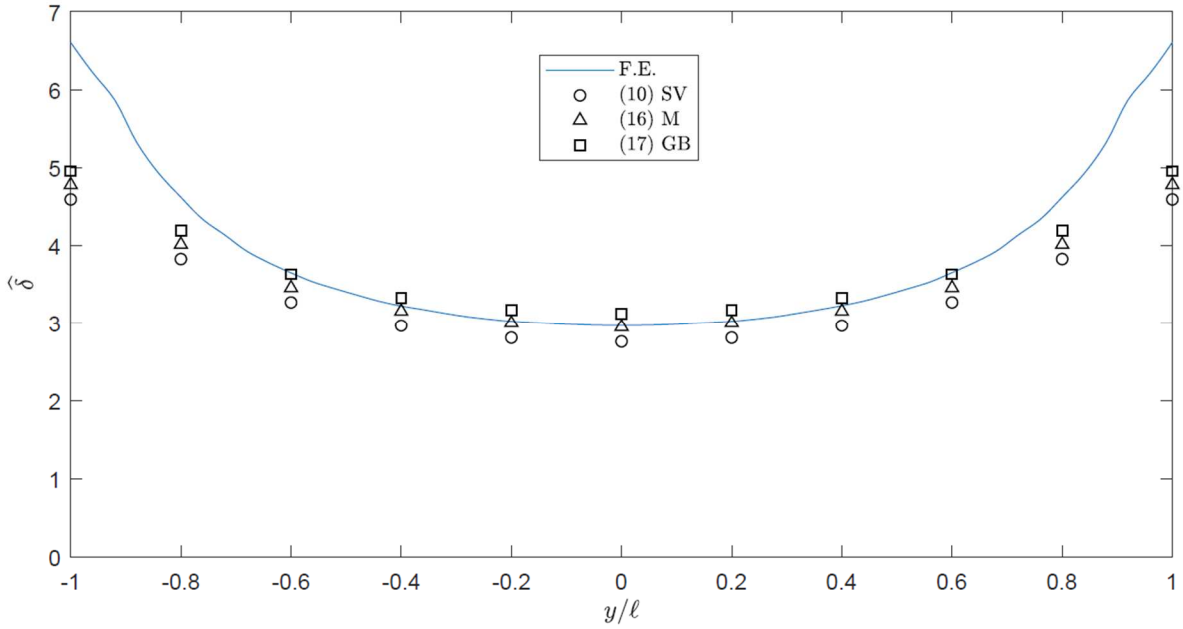

Figure 15 - Comparisons between 3D FE and analytical results across the face width for a half-cosine load distribution at a height corresponding to the pitch radius. Spur gear example.

Finally, the case of helical gears is tackled (Figure 16) for two different helix angles of 10° and 30° with similar node density and boundary conditions while keeping as a reference the normal displacements along the curved intersection between the tooth mid-surface and the base plane. For the smallest helix angle (Fig. 17), the behaviour is similar to that of spur gears and the analytical deflections compare well with the numerical results (similar results have been found for a helix angle of 20°, which are not shown here for the sake of brevity). The thin-slice approach is not as effective for the largest helix angle and, close to the flank edges, substantial deviations are here again observed although the global agreement remains acceptable (Fig. 18).

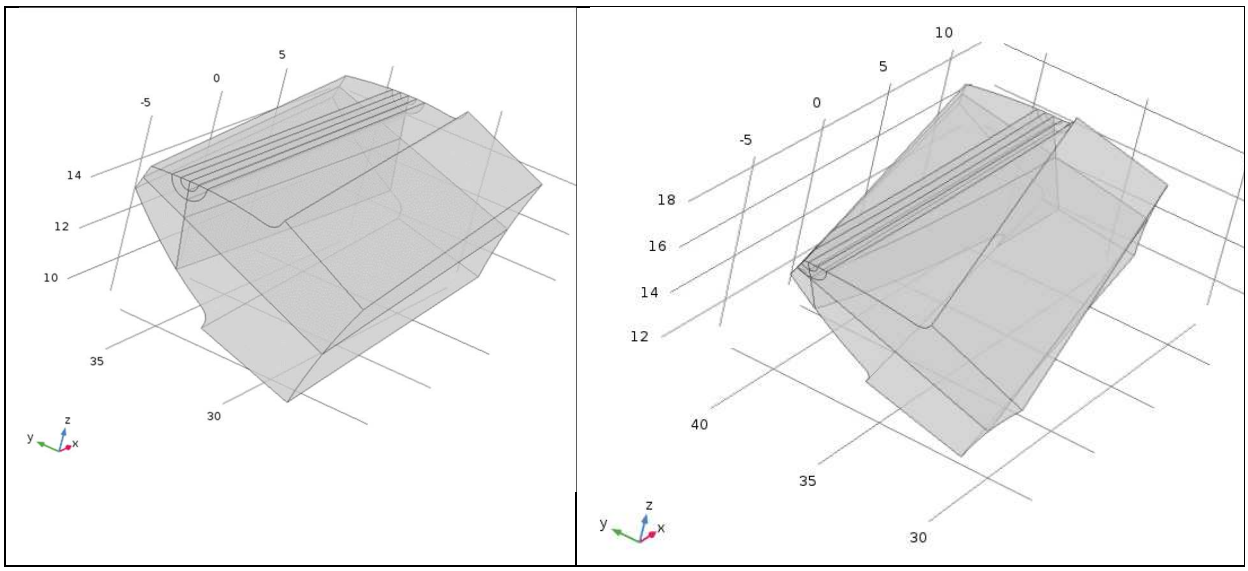

Figure 16 – Finite element models of helical gears.

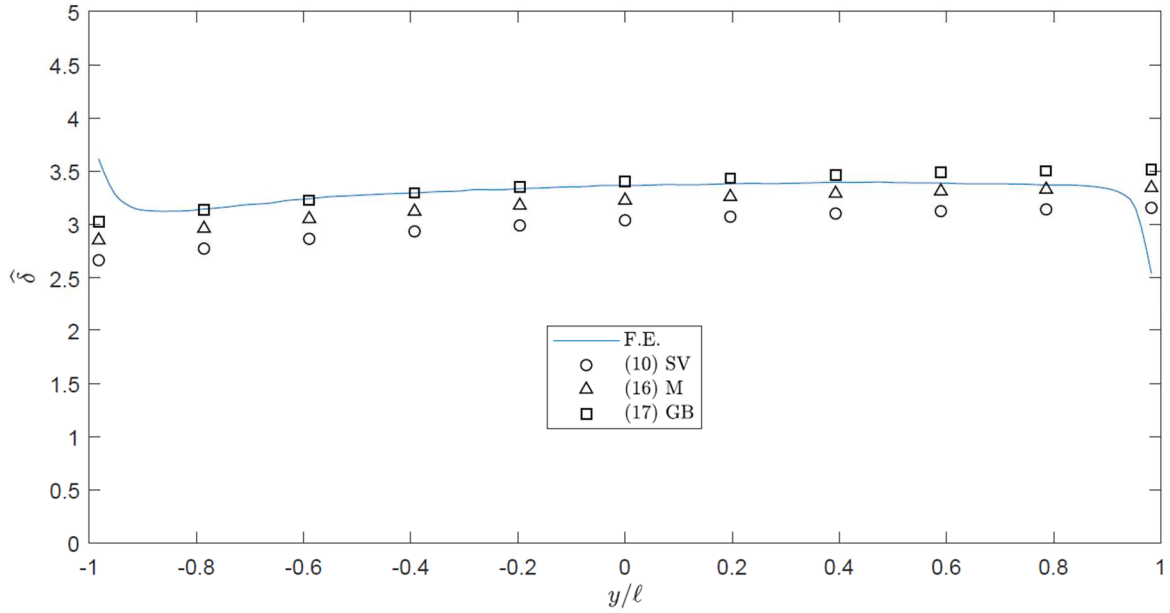

Figure 17 - Comparisons between 3D FE and analytical results at various points along the contact line. Uniform load distribution at the intersection between the tooth flank and the pitch cylinder. Helical gear example ($\beta = 10°$).

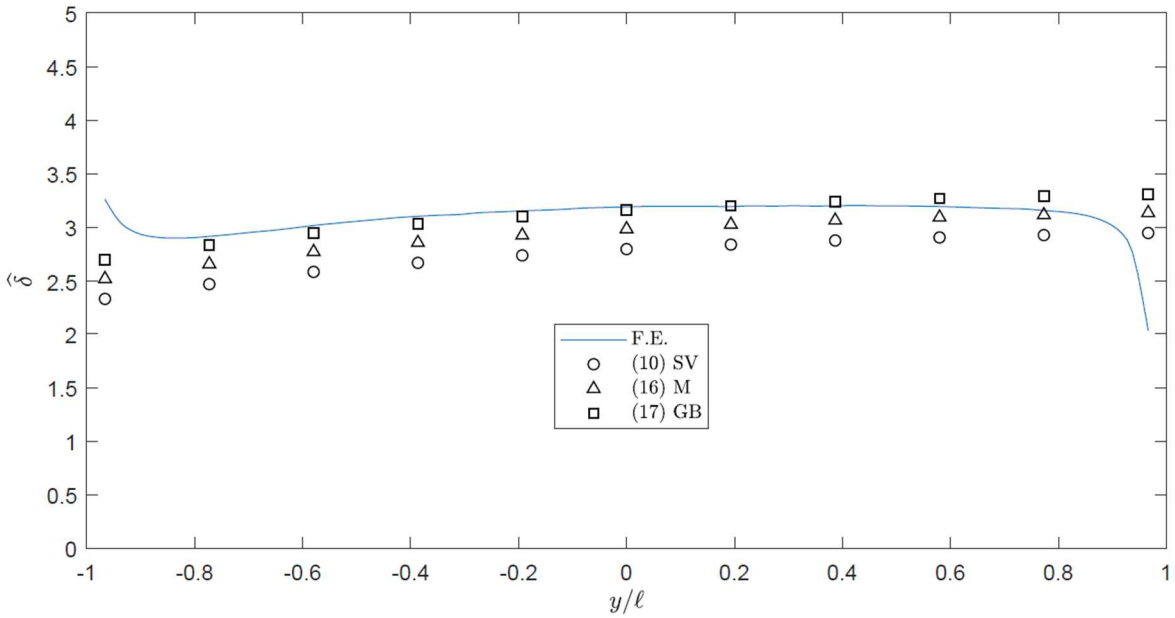

Figure 18 - Comparisons between 3D FE and analytical results at various points along the contact line. Uniform load distribution at the intersection between the tooth flank and the pitch cylinder. Helical gear example ($\beta = 30°$).

3 – Discussion

The vast majority of the deflection equations stem from the hypothesis of two- or three-dimensional semi-infinite elastic media (either half-plane, half-space or infinite slabs) and, for line contacts ($\overline{\ell} >> 1$), it has been proved that their formal differences are mainly due to their respective datum position (implicit or explicit) for vertical displacements, i.e.

a) a set datum depth for WB-SV (10), usually k as defined in Figure 5
b) the slab thickness for M (16), GB (17), which can be made equal to k in gear applications
c) the cylinder centre for J (21) and other related equations in the literature [33-34]
d) for L (6), a 'floating' implicit datum $\overline{z}_L$ (13) depending on the loading conditions whose minimum value, for a precision $\varepsilon = 0.02$, is found to be consistently far larger than the maximum value of $\overline{k}$ for the range of gear modules considered in this paper.

In view of the symmetry in the experimental conditions, the empirical equation P (20) can be affiliated to category c) as the centre of a cylinder pressed against two elastic platens does not experience any vertical displacement [30], [34]. The corresponding orders of magnitude for the contact deflection in Figure 9 and Table 2 are comparable with those found for J (21), thus confirming this hypothesis.

The linear contact deflection (proportional to load) derived from YS –P (19) is clearly apart from all the other equations in the literature, whereas HS (18) seems to be a reasonable estimate of the average contact deflections in gears.

Based on these observations, it can be deduced that the equations in categories c) and d) are generally not suited to gear tooth compliance since, for standard gear geometries, their datum depths often correspond to points outside the teeth that could not be considered as part of the same elastic body. On the other hand, formulae in categories a) and b) appear as more adapted to gears. The hypothesis of a three-dimensional half-space submitted to a finite pressure band is not valid in absolute terms (since the load generally covers the entire tooth face-width) but, interestingly, it still gives good results (Figure 6) providing that relative displacements between the surface and the datum are considered. Based on these formulae relevant for gears, a unique dimensionless expression of the contact deflection for one solid (labelled i here) is therefore proposed under the form:

$$\hat{\delta}_i = \ln\left(2\overline{k}_i\right) + c_0 \qquad (29)$$

where c_0 is a constant whose contribution is, most of the time, rather secondary compared with the logarithmic term (see Table 1).

Considering two contacting solids ($i = 1, 2$), the total compliance is derived from the total dimensionless deflection $\hat{\delta}_T$ as:

$$\frac{\partial \delta_T}{\partial W} = \frac{\partial\left(\Lambda \hat{\delta}_T\right)}{\partial \Lambda}\left(\frac{d\Lambda}{dW}\right) = \frac{\Lambda}{W}\left[\hat{\delta}_T + \Lambda \frac{\partial \hat{\delta}_T}{\partial \Lambda}\right] = \frac{\Lambda}{W}\left[\hat{\delta}_T - 1\right] \qquad (30)$$

where $\hat{\delta}_T = \sum_1^2 \hat{\delta}_i = \ln\left(4\bar{k}_1\bar{k}_2\right) - 2c_0$

Contact stiffness k_h is a key parameter in most gear models and it is determined as the inverse of the contact compliance (30), such that:

$$k_h = k_{ys}\,\frac{2}{\hat{\delta}_T - 1} \qquad (31)$$

where $k_{ys} = \frac{W}{2\Lambda} = \frac{\pi E\left(2\ell\right)}{4\left(1-\nu^2\right)}$ is the linear contact stiffness introduced in [23-29] for a pinion and gear of the same material.

Taking the double of the numerical limits for the relevant formulae in Table 2 in order to account for two contacting solids (hence $2.46 \le \hat{\delta}_T \le 9.36$), it is found that overall:

$$0.24 \le \frac{k_h}{k_{ys}} \le 1.37 \qquad (32)$$

whereas the Hamilton Standard formula leads to a linear stiffness $k_{HS} \approx 0.28 k_{ys}$ so that:

$$0.85 \le \frac{k_h}{k_{HS}} \le 3.5 \qquad (33)$$

Figure 19 shows the range of contact stiffness derived from (31), (32) and (33) for modules between 1 and 8 mm, which confirms these general trends and brings additional information. If $k_{ys} = \pi E\left(2\ell\right)/4\left(1-\nu^2\right)$ could be used as an upper bound for the smaller modules between 1 and 2 mm, it clearly overestimates the contact stiffness for modules above 3 mm (by a factor of more than 2 if one considers the average stiffness). On the other hand, HS (18) more or less always coincides with the lower bound of (31).

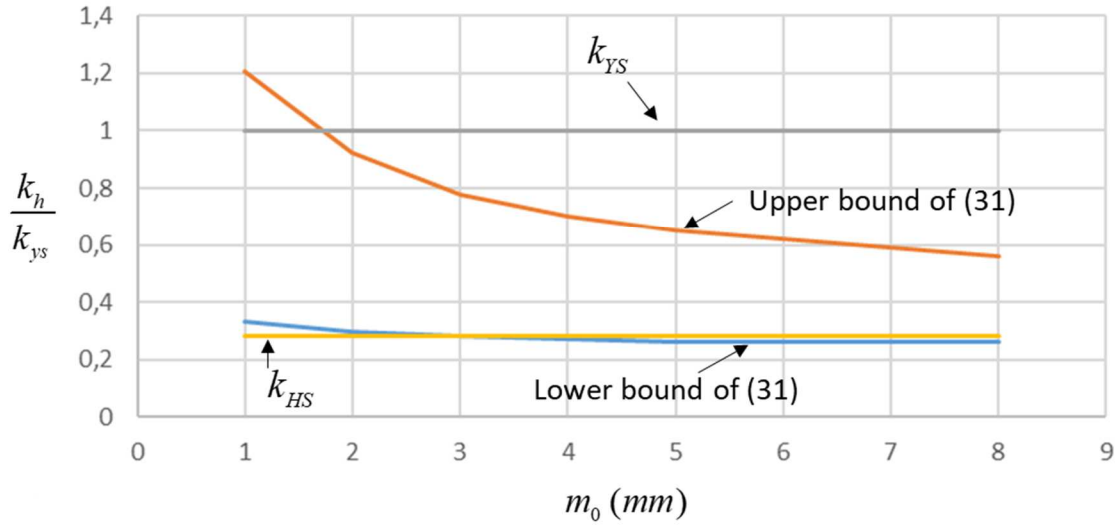

Figure 19 – Comparisons between several contact stiffness models.

The non-linearity of the load-dependent contact stiffness k_h (via $\hat{\delta}_T$) can be appraised by calculating its rate of variation with respect to load given by:

$$\frac{\partial}{\partial W}\left(k_h\right)=2k_{ys}\frac{\partial}{\partial\Lambda}\left(\frac{1}{\hat{\delta}_T-1}\right)\frac{d\Lambda}{dW}=\frac{1}{\Lambda\left(\hat{\delta}_T-1\right)^2}>0 \qquad (34)$$

which, confirms the hardening character of contact stiffness.

4 - Conclusion

A thorough analysis of the classic contact deflection formulae in the literature has been presented in this paper, which, in the authors' opinion, sheds light on the links between apparently very different approaches. A number of results appear as not adapted to gears since they rely on data located outside the teeth or give deflection amplitudes which are far too small because elastic couplings are discarded. A unique expression of the contact deflection and corresponding stiffness is proposed whose structure is close to that derived from (9), (10), (16) and (17), which all compare well with the results obtained using 2D and 3D finite element models. It is noticed, however, that, in a way, the definition of the contact deflection and stiffness for gears depend on how the total displacements are reconstructed by superimposing structural (tooth bending, foundation) and contact deflections. The classic methodology, that dates back to the early works of Weber [1], consists in setting contact displacements to zero at the intersection between the base plane and the tooth mid-surfaces or centre lines so that only structural displacements are taken into account at these points. The results in this paper also suggest that the influence of contact deflections does not necessarily

vanish at the reference point at depth *k*. It can therefore be inferred that the overall mesh compliance can be underestimated by this superposition method and, as proposed by Sainsot [35], it could be more accurate to set a nil contact displacement on the coast side of the teeth. Finally, for three-dimensional models, it has been shown that a classic thin-slice representation with independent elements distributed along the contact lines can effectively represent contact compliance or stiffness. Deviations are noted when the deformed shape is distorted (mainly near the free edges) and elastic couplings cannot be ignored. Even so, the deflections in the central part of the contact lines are correctly reproduced.

References:

[1] C. Weber, The Deflection of Loaded Gears and the Effects on their Load Carrying Capacity, Dept. of Scientific and Industrial Research, Sponsored Research, Germany, Report n° 3, 1949.

[2] C. Weber, K. Banaschek, Formänderung und Profilrücknahme bei Gerad-und Schrägverzahnten Antriebstechnik, Vieweg, Braunschweig, Vol. 11, 1953.

[3] A. Y. Attia, Deflection of Spur Gear Teeth Cut in Thin Rims, J. Manuf. Sci. Eng. **86**(4) (1964) 333-341, doi:10.1115/1.3670554

[4] K. Umezawa, 1972, Deflections and moments due to a concentrated load on a rack-shaped cantilever plate with finite width for gears, Bulletin of JSME, **15**(79) (1972) 116-130. doi.org/10.1299/jsme1958.15.116

[5] E. Yau, H.R. Busby, D.R. Houser, A Rayleigh-Ritz approach to modeling, bending and shear deflections of gear teeth, Computers & Structures, **50** (5) (1994) 705-713. doi: 10.1016/0045-7949(94)90429-4

[6] R.W. Cornell, Compliance and stress sensitivity of spur gear teeth, Journal of Mechanical Design, **103**(2) (1981) 447-459. doi:10.1115/1.3254939

[7] P. Sainsot, P. Velex, O. Duverger, Contribution of gear body to tooth deflections-a new bidimensional analytical formula. J. Mech. Des. **126**(4) (2004) 748-752. doi.org/10.1115/1.1758252

[8] S. Du, R.B. Randall, D.W. Kelly, Modelling of spur gear mesh stiffness and static transmission error, Proceedings of the Institution of Mechanical Engineers, Part C: Journal of Mechanical Engineering Science, **212**(4) (1998) 287-297. doi.org/10.1243/0954406981521222

[9] J. Wang, I. Howard, The torsional stiffness of involute spur gears, Proceedings of the Institution of Mechanical Engineers, Part C: Journal of Mechanical Engineering Science, **218**(1) (2004) 131-142. doi.org/10.1243/095440604322787009

[10] A. Palermo, D. Mundo, R. Hadjit, W. Desmet, Multibody elements for spur and helical gear meshing based on detailed three-dimensional contact calculations. Mechanism and Machine Theory, **62**(2013) 13-30. doi.org/10.1016/j.mechmachtheory.2012.11.006

[11] A. Fernandez Del Rincon, F. Viadero, M. Iglesias, P. Garcia, A. de-Juan, R. Sancibrian, A model for the study of meshing stiffness in spur gear transmissions, Mechanism and Machine Theory **61** (2013) 30-58. doi.org/10.1016/j.mechmachtheory.2012.10.008

[12] N. L. Pedersen, M. F. Jorgensen, On gear tooth stiffness evaluation, Computers and Structures, **135** (2014) 109-117. doi.org/10.1016/j.compstruc.2014.01.023

[13] X. Gu, P. Velex, P. Sainsot, J. Bruyère, Analytical investigations on the mesh stiffness function of solid spur and helical gears, Journal of Mechanical Design, **137**(6) (2015), 6 pages. doi.org/10.1115/1.4030272

[14] C.G. Cooley, C. Liu, X. Dai, R.G. Parker, Gear tooth mesh stiffness: A comparison of calculation approaches, *Mechanism and Machine Theory*, **105** (2016) 540-553. doi.org/10.1016/j.mechmachtheory.2016.07.021

[15] C. Xie, L. Hua, J. Lan, X. Han, X.Wan, X. Xiong, Improved analytical models for mesh stiffness and load sharing ratio of spur gears considering structure coupling effect, Mechanical Systems and Signal Processing, **111**(2018) 331-347. doi.org/10.1016/j.ymssp.2018.03.037

[16] K.L. Johnson, Contact Mechanics, Cambridge University Press, 2003

[17] J. Boussinesq, Application dès potentiels a l'étude de l'équilibre et du mouvement des solides élastiques, Gauthier-Villars, 1885.

[18] G. Lundberg, Elastische Berührung zweier Halbraüme, Forsch. Geb. Ingenieurwes., **10** (5) (1939) 201–211.

[19] H. Moes, Lubrication and Beyond, University of Twente Lecture Notes code 115531. University of Twente, Enschede, The Netherlands, 2000.

[20] P. Meijers, P. The contact problem of a rigid cylinder on an elastic layer. Applied Scientific Research, **18**(1) (1968) 353-383.

[21] J.A. Greenwood, C. Putignano, M. Ciavarella, A Greenwood & Williamson theory for line contact, Wear, **270**(3–4) (2011) 332-334. doi.org/10.1016/j.wear.2010.11.002

[22] J.A. Greenwood, J.R. Barber, Indentation of an elastic layer by a rigid cylinder, International Journal of Solids and Structures, **49**(21) (2012) 2962-2977. doi.org/10.1016/j.ijsolstr.2012.05.036

[23] D.C.H. Yang, Z. S. Sun, A rotary model for spur gear dynamics, J. Mech., Trans., and Automation, **107**(4) (1985) 529-535. doi.org/10.1115/1.3260759

[24] N. Sarkar, R.E. Ellis, T.N. Moore, Backlash detection in geared mechanisms: modeling, simulation, and experimentation, Mechanical Systems and Signal Processing, **11**(3) (1997) 391-408. doi.org/10.1006/mssp.1996.0082

[25] F. Chaari, T. Fakhfakh, M. Haddar, Analytical modelling of spur gear tooth crack and influence on gearmesh stiffness, European Journal of Mechanics-A/Solids, **28**(3) (2009) 461-468. doi.org/10.1016/j.euromechsol.2008.07.007

[26] Z. Chen, Y. Shao, Dynamic simulation of spur gear with tooth root crack propagating along tooth width and crack depth, Engineering Failure Analysis, **18**(8) (2011) 2149-2164. doi.org/10.1016/j.engfailanal.2011.07.006

[27] X. Liang, M.J. Zuo, M. Pandey, Analytically evaluating the influence of crack on the mesh stiffness of a planetary gear set, Mechanism and Machine Theory, **76** (2014) 20-38. doi.org/10.1016/j.mechmachtheory.2014.02.001

[28] Z. Chen, W. Zhai, Y. Shao, K. Wang, G. Sun, Analytical model for mesh stiffness calculation of spur gear pair with non-uniformly distributed tooth root crack, Engineering Failure Analysis, **66** (2016) 502-514. doi.org/10.1016/j.engfailanal.2016.05.006

[29] V. L. Popov, Contact Mechanics and Friction –Physical Principles and Applications, Springer, 2010. doi.org/10.1007/978-3-642-10803-7

[30] A. Palmgren, Ball and roller bearing engineering, 3rd edition, Philadelphia, SKF Industry Inc., 1959.

[31] D.L. Seager, Some elastic effects in helical gears, PhD Cambridge University, 209 p, 1967.

[32] M. Ajmi, M., P. Velex, A model for simulating the quasi-static and dynamic behaviour of solid wide-faced spur and helical gears, Mechanism and Machine Theory, **40** (2) (2015) 173-190. doi: 10.1016/j.mechmachtheory.2003.06.001

[33] B.N. Norden, On the compression of a cylinder in contact with a plane surface, Report NBSIR 73-243, Institute for Basic Standards, National Bureau of Standards, Washington DC, 61 pages, 1973.

[34] K. Nikpur, R. Gohar, Deflexion of a roller compressed between platens, Tribology International, **8**(1) (1975) 2-8.

[35] P. Sainsot, Analyse du contact entre dentures d'engrenages cylindriques de réducteurs, PhD, INSA Lyon, 1989.

[36] I.S. Gradshteyn, I.M. Ryzhik, Table of Integrals, Series and Products', 7th edition, Elsevier, Academic Press, 2007.

Annex

1 – General expressions for vertical displacements in a half-space loaded by a pressure distribution as shown in Figure 2.

Following Boussinesq [17], the normalised vertical displacement $\hat{w}(0,\overline{y},\overline{z})$ at any point on the plane of symmetry $\overline{x}=0$ of an elastic homogeneous half –space submitted to a pressure distribution semi-elliptical in the $(O,\mathbf{x})$ direction and uniform over $-\overline{\ell}\le\overline{y}\le\overline{\ell}$ in the $(O,\mathbf{y})$ can be expressed as:

$$\hat{w}(0,\overline{y},\overline{z})=\hat{w}_1(0,\overline{y},\overline{z})+\hat{w}_2(0,\overline{y},\overline{z}) \qquad \text{(A)}$$

where

$$\hat{w}_1(0,\overline{y},\overline{z})=\frac{1}{\pi}\int_{-1}^{+1}\int_{-\overline{\ell}}^{+\overline{\ell}}\frac{\sqrt{1-\overline{x}'^2}}{\sqrt{\overline{x}'^2+\left(\overline{y}'-\overline{y}\right)^2+\overline{z}^2}}\,d\overline{y}'d\overline{x}'$$

$$\hat{w}_2(0,\overline{y},\overline{z})=\frac{1}{2\pi(1-\nu)}\overline{z}^2\int_{-1}^{+1}\int_{-\overline{\ell}}^{+\overline{\ell}}\frac{\sqrt{1-\overline{x}'^2}}{\left(\overline{x}'^2+\left(\overline{y}'-\overline{y}\right)^2+\overline{z}^2\right)^{3/2}}\,d\overline{y}'d\overline{x}'$$

$$\overline{x}=\frac{x}{b},\ \overline{y}=\frac{y}{b},\ \overline{z}=\frac{z}{b},\ \overline{\ell}=\frac{\ell}{b},\ \hat{w}=\frac{w}{\Lambda}$$

$$\Lambda=\frac{1-\nu^2}{E}P_0b=2\frac{1-\nu^2}{E}\frac{W}{\pi(2\ell)}=\frac{b^2}{4R}$$

A first integration with respect to $\overline{y}'$ gives :

$$\hat{w}_1(0,\overline{y},\overline{z})=\frac{1}{\pi}\int_{-1}^{+1}\sqrt{1-\overline{x}'^2}\,\ln\left[\frac{\left(\overline{\ell}-\overline{y}\right)+\sqrt{\overline{x}'^2+\left(\overline{\ell}-\overline{y}\right)^2+\overline{z}^2}}{-\left(\overline{\ell}+\overline{y}\right)+\sqrt{\overline{x}'^2+\left(\overline{\ell}+\overline{y}\right)^2+\overline{z}^2}}\right]d\overline{x}' \qquad \text{(B-1)}$$

$$\hat{w}_2(0,\overline{y},\overline{z})=\frac{1}{\pi(1-\nu)}\overline{z}^2\int_{-1}^{+1}\sqrt{1-\overline{x}'^2}\left[\begin{array}{l}\dfrac{\overline{\ell}-\overline{y}}{\left(\overline{x}'^2+\overline{z}^2\right)\sqrt{\overline{x}'^2+\left(\overline{\ell}-\overline{y}\right)^2+\overline{z}^2}}\\ +\dfrac{\overline{\ell}+\overline{y}}{\left(\overline{x}'^2+\overline{z}^2\right)\sqrt{\overline{x}'^2+\left(\overline{\ell}+\overline{y}\right)^2+\overline{z}^2}}\end{array}\right]d\overline{x}' \qquad \text{(B-2)}$$

2 - Displacement at the surface $\bar{z}=0$ *such that* $\bar{\ell}-|\bar{y}|>>x'$ *(not too close to the contact edges)*

$$\hat{w}_2(0,\bar{y},\bar{z})=0 \qquad \text{(C-1)}$$

and

$$\hat{w}_1(0,\bar{y},0)=\frac{1}{\pi}\int_{-1}^{+1}\sqrt{1-\bar{x}'^2}\,\ln\left[\frac{\left(\bar{\ell}-\bar{y}\right)+\sqrt{\bar{x}'^2+\left(\ell-\bar{y}\right)^2}}{-\left(\bar{\ell}+\bar{y}\right)+\sqrt{\bar{x}'^2+\left(\ell+\bar{y}\right)^2}}\right]d\bar{x}' \qquad \text{(C-2)}$$

Assuming that $\bar{\ell}-|\bar{y}|>>x'$, (C-2) is transformed into :

$$\hat{w}(0,\bar{y},0)=\frac{1}{\pi}\int_{-1}^{+1}\sqrt{1-\bar{x}'^2}\,\ln\left[\frac{\left(\bar{\ell}-\bar{y}\right)+\sqrt{\left(\bar{\ell}-\bar{y}\right)^2}}{-\left(\bar{\ell}+\bar{y}\right)+\left(\bar{\ell}+\bar{y}\right)\sqrt{\dfrac{\bar{x}'^2}{\left(\bar{\ell}+\bar{y}\right)^2}+1}}\right]d\bar{x}' \;\square\; \frac{1}{\pi}\int_{-1}^{+1}\sqrt{1-\bar{x}'^2}\,\ln\left[\frac{4\left(\bar{\ell}^2-\bar{y}^2\right)}{\bar{x}'^2}\right]d\bar{x}'$$

(C-3)

Introducing a new variable θ such that : $\bar{x}'=\sin\theta$ and $d\bar{x}'=\cos\theta\,d\theta$, one obtains:

$$\hat{w}(0,\bar{y},0)=\frac{2}{\pi}\ln\left[4\left(\bar{\ell}^2-\bar{y}^2\right)\right]\int_0^{\pi/2}\cos^2\theta d\theta-\frac{4}{\pi}\int_0^{\pi/2}\cos^2\theta\ln\left(\sin\theta\right)d\theta \qquad \text{(C-4)}$$

which, integrated using BI (305) (8) in [36] leads to:

$$\hat{w}(0,\bar{y},0)=\frac{1}{2}\ln\left[4\left(\bar{\ell}^2-\bar{y}^2\right)\right]-\frac{4}{\pi}\left[-\frac{\pi}{8}\left(1+\ln 4\right)\right]=\ln\left[2\sqrt{\bar{\ell}^2-\bar{y}^2}\right]+\frac{1}{2}\left(1+\ln 4\right) \qquad \text{(C-5)}$$

re-written as:

$$\hat{w}(0,\bar{y},0)\;\square\;\ln\left(2\bar{\ell}\right)+\frac{1}{2}\ln\left(1-\left(\frac{\bar{y}}{\bar{\ell}}\right)^2\right)+1.193 \qquad \text{(C-6)}$$

3- Displacement at the surface $\bar{z}=0$ *at the contact edges* $\bar{y}=\pm\bar{\ell}$

From (C-2), one obtains:

$$\hat{w}(0,\overline{\ell},0)=\frac{2}{\pi}\int_0^{+1}\sqrt{1-\overline{x}'^2}\,\ln\left[\frac{\sqrt{\overline{x}'^2}}{-\left(2\overline{\ell}\right)+\sqrt{\overline{x}'^2+\left(2\overline{\ell}\right)^2}}\right]d\overline{x}' \qquad \text{(D-1)}$$

which, using the same change of variable in (C-4) and supposing that $\left(\frac{\overline{x}}{\overline{\ell}}\right)^2 << 1$ gives:

$$\hat{w}(0,\overline{\ell},0)=\frac{2}{\pi}\left[\int_0^{+\frac{\pi}{2}}\cos^2\theta\ln\left(4\overline{\ell}\right)d\theta-\int_0^{+\frac{\pi}{2}}\cos^2\theta\ln(\sin\theta)\,d\theta\right] \qquad \text{(D-2)}$$

The structure of (D-2) is similar to that of (C-4) and can be integrated the same way, leading to:

$$\hat{w}(0,\overline{\ell},0)=\frac{1}{2}\ln\left(2\overline{\ell}\right)+0.943 \qquad \text{(D-3)}$$

It can be verified that the result is the same at $\overline{y}=-\overline{\ell}$.

4 - Displacements at depth $\overline{z}\neq 0$ *and assuming that* $\sqrt{\left(\overline{\ell}+\overline{y}\right)^2+\overline{z}^2} >> x'$

The first displacement component in (A) is transformed into

$$\hat{w}_1(0,\overline{y},\overline{z})=\frac{1}{2}\ln\left[\frac{\sqrt{\left(\overline{\ell}-\overline{y}\right)^2+\overline{z}^2}+\left(\overline{\ell}-\overline{y}\right)}{\sqrt{\left(\overline{\ell}+\overline{y}\right)^2+\overline{z}^2}-\left(\overline{\ell}+\overline{y}\right)}\right]-\frac{1}{\pi}\int_{-\frac{\pi}{2}}^{+\frac{\pi}{2}}\cos^2\theta\ln\left[1+A\sin^2\theta\right]d\theta \qquad \text{(E-1)}$$

with $\quad A=\dfrac{\left[\sqrt{\left(\overline{\ell}+\overline{y}\right)^2+\overline{z}^2}+\left(\overline{\ell}+\overline{y}\right)\right]}{2\overline{z}^2\sqrt{\left(\overline{\ell}+\overline{y}\right)^2+\overline{z}^2}}$

Integration using BI (309) (15) in [36] gives:

$$\hat{w}_1(0,\overline{y},\overline{z})=\frac{1}{2}\ln\left[\frac{\sqrt{\left(\overline{\ell}-\overline{y}\right)^2+\overline{z}^2}+\left(\overline{\ell}-\overline{y}\right)}{\sqrt{\left(\overline{\ell}+\overline{y}\right)^2+\overline{z}^2}-\left(\overline{\ell}+\overline{y}\right)}\right]-\left[\ln\left[\frac{1+\sqrt{1+A}}{2}\right]+\frac{1}{2}\frac{1-\sqrt{1+A}}{1+\sqrt{1+A}}\right] \qquad \text{(E-2)}$$

The second displacement $\hat{w}_2(0,\overline{y},\overline{z})$ in (A), which is not nil in this case, reads:

$$\hat{w}_2(0,\bar{y},\bar{z}) = \frac{1}{2\pi(1-\nu)}\left[\frac{\bar{\ell}-\bar{y}}{\sqrt{\left(\bar{\ell}-\bar{y}\right)^2+\bar{z}^2}}+\frac{\bar{\ell}+\bar{y}}{\sqrt{\left(\bar{\ell}+\bar{y}\right)^2+\bar{z}^2}}\right]\int_{-1}^{+1}\sqrt{1-\bar{x}'^2}\,\frac{1}{\left(1+\frac{\bar{x}'^2}{\bar{z}^2}\right)}d\bar{x}' \quad \text{(E-3)}$$

Assuming that $\frac{\bar{x}'^2}{\bar{z}^2} << 1$, the integral is re-written as:

$$\int_{-1}^{+1}\sqrt{1-\bar{x}'^2}\left(1-\frac{\bar{x}'^2}{\bar{z}^2}\right)d\bar{x}' = \int_{-\frac{\pi}{2}}^{+\frac{\pi}{2}}\cos^2\theta\left(1-\frac{1}{\bar{z}^2}\sin^2\theta\right)d\theta \qquad \text{(E-4)}$$

which, after integration, gives:

$$\hat{w}_2(0,\bar{y},\bar{z}) = -\frac{1}{2(1-\nu)}\left[\frac{\bar{\ell}-\bar{y}}{\sqrt{\left(\bar{\ell}-\bar{y}\right)^2+\bar{z}^2}}+\frac{\bar{\ell}+\bar{y}}{\sqrt{\left(\bar{\ell}+\bar{y}\right)^2+\bar{z}^2}}\right]\left(\bar{z}^2-\bar{z}\sqrt{1+\bar{z}^2}\right) \quad \text{(E-5)}$$

The total displacement at depth $\bar{z}\neq 0$ is finally derived by adding (E-2) and (E-5) which leads to equation (8).

5 – Relative displacement between the surface and at depth $\bar{z}\neq 0$ *and assuming that* $\left(\frac{\bar{z}}{\bar{\ell}\pm\bar{y}}\right)^2 << 1$ *(central part of the contact width)*

In these conditions, it can be shown that A in (E-1) and (E-2) becomes:

$$A \approx \frac{1}{\bar{z}^2} \qquad \text{(F-1)}$$

and that (E-1) and (E-2) can be simplified as:

$$\hat{w}_1(0,\bar{y},\bar{z}) \approx \ln\left(2\bar{\ell}\right)+\frac{1}{2}\ln\left(1-\frac{\bar{y}^2}{\bar{\ell}^2}\right)+\ln(2)+\frac{1}{2}-\ln\left(\bar{z}\left(1+\sqrt{1+\frac{1}{\bar{z}^2}}\right)\right)+\bar{z}^2\left(1-\sqrt{1+\frac{1}{\bar{z}^2}}\right) \qquad \text{(F-2)}$$

$$\hat{w}_2(0,\bar{y},\bar{z}) \approx -\frac{1}{(1-\nu)}\bar{z}^2\left(1-\sqrt{1+\frac{1}{\bar{z}^2}}\right) \qquad \text{(F-3)}$$

The total vertical displacement is deduced as:

$$\hat{w}(0,\overline{y},\overline{z}) \approx \ln\left(2\overline{\ell}\right)+\frac{1}{2}\ln\left(1-\frac{\overline{y}^2}{\overline{\ell}^2}\right)+1.193-\ln\left(\overline{z}\left(1+\sqrt{1+\frac{1}{\overline{z}^2}}\right)\right)-\frac{\nu}{1-\nu}\overline{z}^2\left(1-\sqrt{1+\frac{1}{\overline{z}^2}}\right) \tag{F-4}$$

finally re-written as:

$$\hat{w}(0,\overline{y},\overline{z}) \approx \hat{w}(0,\overline{y},0)-\ln\left(\overline{z}\left(1+\sqrt{1+\frac{1}{\overline{z}^2}}\right)\right)-\frac{\nu}{1-\nu}\overline{z}^2\left(1-\sqrt{1+\frac{1}{\overline{z}^2}}\right) \tag{F-5}$$

which corresponds to (9) in the text.

Z	m_0 (mm)	α_0 (°)	β (°)	h_a	h_f	x		p_0 (GPa)	b (mm)
25	2	20	0 10 30	1	1.25	0		1.34 1.30 1.23	0.12 0.12 0.16

Table 3 – Gear data and loading conditions